nature water

Article

https://doi.org/10.1038/s44221-022-00003-2

Nanosecond bacteria inactivation realized by locally enhanced electric field treatment

In the format provided by the authors and unedited

Table of Contents

1. Additional methods

1.1. Chip fabrication and pretreatment

1.2. Calculation of the applied electric field

2. Additional discussion

2.1. Energy consumption in nanosecond LEEFT

2.2. Water ionization and bubble formation in LEEFT

2.3. Electrochemical oxidation in nanosecond LEEFT

2.4. Membrane charging and electroporation process

2.5. Membrane charging process when not contacting the nanowedge

3. Supplementary figures

Figure S1. Photos of the chip and the experimental setup.

Figure S2. A schematic of the double staining method with SYTOX Green and PI stain.

Figure S3. Side-by-side comparison of the optical microscopy images and SEM images for bacteria inactivation by LEEFT using different treatment conditions.

Figure S4. Simulation of the enhanced electric field of nanotip structures on chip.

Figure S5. The area of interest for CEFT and LEEFT.

Figure S6. Relative energy consumption of 20 ns pulses at different applied electric field.

Figure S7. PI fluorescence intensity indicating quick pore closure in the cells located at the tips of the non-connected nanowedges.

Figure S8. The stack fluorescence microscopy image of DCFH-DA and PI stained bacteria.

Figure S9. Analysis and microscopy imaging of cell membrane peroxidation.

Figure S10. Electroporation process and membrane charging speed analysis.

Figure S11. The normalized TMV changed with charging time.

Figure S12. Waveform of a single electrical pulse.

1. Additional methods

1.1. Chip fabrication and pretreatment

To fabricate the gold nanowedges, a layer of electron beam resist PMMA A6 was spin-coated on the surface of a glass wafer substrate. Then, the substrate was exposed using an electron beam lithography system (Elionix ELS-G100). After development, a thin layer of gold (200 nm) was deposited using an e-beam evaporator (Denton Explorer). The unwanted gold was removed by a lift-off method using acetone, leaving the gold nanowedges on the substrate. After the nanowedges were fabricated, the 300 nm thick bulk gold electrodes with 25 or 50 μm electrode separation gap were fabricated using a similar procedure except that photolithography was used rather than e-beam lithography. A layer of photoresist (NR9-1500py) was first spin coated on the substrate, then exposed by photolithography (Heidelberg MLA150), and the gold was deposited by e-beam evaporator and lift-off method.

To achieve bacteria immobilization on the chip, the fabricated chips were first washed with 5% bleach for 30 min, rinse with DI water, washed with 30% H_2O_2 for 1 hour, stored in DI water overnight,[1] and then dried in oven before treatment. The dried chips were then coated with positively charged poly-L-lysine (0.01%, mw 150,000-300,000; Sigma-Aldrich) for bacteria immobilization. Specifically, poly-L-lysine and 2 M borate buffer was first mixed at 1:1, then about 50 μL of the mixture was added onto the center of a dried chip, covering the gap between the two electrodes. After 3 hours of coating at room temperature, the chips were rinsed with DI water and dried in 60 ℃ for 20 min. The coated chips were stored in 4 ℃ to avoid coating layer degradation. Poly-L-lysine is a positively charged polymer, which can immobilize the negatively charged bacteria on the chip surface. To reuse the chips after experiments, repeat the wash and coating steps.

1.2. Calculation of the applied electric field

The applied electric field used in the figures and discussion is the background electric field, which is calculated by the equation, $EF = V / d$, where V is the applied voltage and d is the distance separating the positive/negative electrodes. Since the electrode separation distance is subject to change in other studies and in real applications, same applied voltage may yield very different electric field. Therefore, the background electric field is widely used in electric field treatment to represent the applied treatment strength. For LEEFT, the electric filed at the tip (E_{tip}) is enhanced roughly estimated by **Equation S1**:

$$E_{\mathrm{tip}} = a \cdot \frac{L_{\mathrm{nanowedge}}}{D_{\mathrm{nanowedge}}} \cdot E_{\mathrm{background}} \quad \text{(S1)}$$

where $E_{\mathrm{background}}$ is the background electric field, $L_{\mathrm{nanowedge}}$ and $D_{\mathrm{nanowedge}}$ is the length and width of the nanowedge, and a is a constant.[2] The exact electric field at the nanowedge tip is affected by some factors, such as the exact shape and material of the nanowedge. Therefore, using the background electric field to represent the applied treatment strength is more general, and makes it more convenient to compare with other studies.

2. Additional discussion

2.1. Energy consumption in nanosecond LEEFT

For nanosecond LEEFT, applying a stronger electric field can greatly reduce energy consumption (**Figure S6**). It is because by slightly increasing the applied electric field, the effective treatment time can be shortened by several orders of magnitude (**Figure 2d**). This property is different from the chemical-based antimicrobial methods relying on oxidation, where increasing the chemical dosage only allows a similar scale of treatment time decrease, so that the product of dosage and time (*i.e.*, the CT value) remains similar for a certain disinfection efficiency.[3] It can be explained by the inherent mechanism difference between electroporation and oxidation. For electroporation, the cells cannot be perforated if the electric field does not reach a threshold, no matter how long the electrical pulse is and how many pulses are applied. However, once pores are induced by a strong electric field, a short effective treatment time is sufficient to inactive the bacteria, which can reduce the energy consumption by several orders of magnitude.

2.2. Water ionization and bubble formation in LEEFT

There should be no water ionization events causing cell inactivation, since the breakdown strength of water is higher than 2 MV/cm with the pulse width <50 ns,[4, 5] which is much higher than the highest applied electric field in this work (55 kV/cm) and the nano-enhanced electric field at the nanowedge tips (<1000 kV/cm). Bubbles were only formed under very strong treatment conditions where severe oxidative stress has already been detected (denoted by * in **Figure 3b**). In this study, there was no bubble formation under 20 ns pulses even at 55 kV/cm.

2.3. Electrochemical oxidation in nanosecond LEEFT

Nanosecond pulses induce less oxidative stress than longer pulses (**Figure 3b**), meaning that the ultrashort pulses are less likely to induce electrochemical reactions under the same voltage and

duty cycle. Although electrochemical reactions may cause more bacteria inactivation, they raise problems including water splitting and generating disinfection by-products (DBPs), thus deteriorating the water quality. With nanosecond pulses, a stronger electric field and higher frequencies could be applied to achieve more efficient bacteria inactivation, while maintaining pristine electroporation, eliminating unwanted side reactions, and minimizing DBP generation. Ultrafast nanosecond pulses are also safer to operate, which makes the approach more applicable for real-world water disinfection applications.

2.4. Membrane charging and electroporation process

The electroporation processes are shown in **Figure S10a**. When the cell is exposed to an external electric field E, the charged ions in the cytoplasm and extracellular medium will migrate and accumulate at the two sides of the membrane, generating an induced TMV (ΔV). When the TMV reaches a certain threshold, water molecules penetrate the membrane, generating a water column and the hydrophobic pore. Then, the lipids rearrange their head group toward the water column, generating the hydrophilic pore. Charging the cell membrane by ions is like charging a capacitor in a circuit, where C is the membrane capacitance, and R_i, R_e, R_m are the resistance of the cytoplasm, extracellular medium, and the membrane (**Figure S10b**).

The TMV induced by the external electric field (ΔV) is given in **Equation S2**:[6]

$$\Delta V = f_s r E cos\theta \left[1 - exp\left(-\frac{t}{\tau}\right)\right] \quad \text{(S2)}$$

where f_s is a factor related to the electric field and properties of the cell and medium, r is the cell radius, E is the external electric field strength, θ is the angle between the direction of electric field and the point of interest, t is the pulse width, and τ is the RC time constant of the membrane, which is the time required to charge the membrane to 63.2% of the maximum possible TMV. The membrane charging constant τ is further determined by **Equation S3**:[6]

$$\tau = \frac{rC_{\mathrm{m}}}{\left(\frac{2\sigma_{\mathrm{e}}\sigma_{\mathrm{i}}}{2\sigma_{\mathrm{e}}+\sigma_{\mathrm{i}}}\right)+\frac{r}{d}\sigma_{\mathrm{m}}} \quad \text{(S3)}$$

where r is the cell radius, C_{m} is the surface capacitance of the membrane, σ_{i}, σ_{e}, and σ_{m} are the conductivities of the cytoplasm, the extracellular medium, and the membrane, respectively, and d is the thickness of membrane. According to the values reported in literature, the f_{s}, σ_{i}, σ_{m}, C_{m}, d, and r are 1.5, 0.2 S/m, 5×10^{-6} S/m, 0.01 F/m^2, 50 nm, and 0.5 μm, respectively.[6] The relationship between the membrane charging constant τ and the extracellular medium conductivity σ_{e} is shown in **Figure S10c**. The charging constant increases with the decrease of conductivity, meaning that longer time is needed to charge the membrane when the extracellular medium conductivity is low. The dependence of the membrane charging percentage on the pulse width under different medium conductivities is shown in **Figure S10d**. Tens of nanoseconds can only charge the membrane to <50%, especially under low conductivities. The conductivities of DI water, tap water, and juice are around 5×10^{-5}, 1×10^{-2}, and 3×10^{-1} S/m, respectively.[7]

2.5. Membrane charging process when not contacting the nanowedge

For the cells not directly contacting the nanowedge tip, the membrane still needs to be charged by the ions in the medium between the cell and the tip. In this case, the charging speed will be affected by both the strength of the locally enhanced electric field, which is determined by the distance of the cells away from the nanowedge tips, and the conductivity of the medium. When the cells are very close to the nanowedge tips (*e.g.*, less than a few hundred nanometers) and the medium conductivity is not very low, inactivation in nanoseconds may still be possible. Nevertheless, the direct cell-nanowedge contact guarantees the fastest membrane charging, which is critical for the nanosecond cell electroporation and inactivation in LEEFT.

3. Supplementary figures

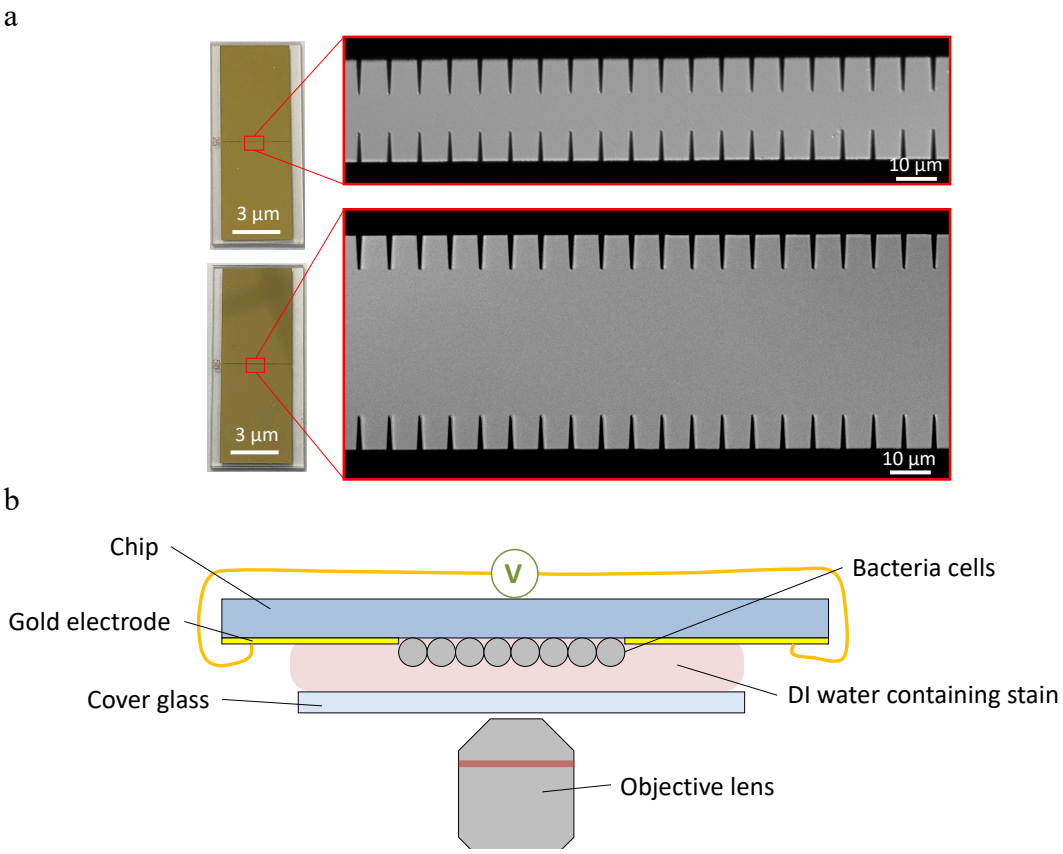

Figure S1. Photos of the chip and the experimental setup. (a) Digital photos and optical microscopy images of the lab-on-a-chip with 20 µm or 50 µm gap between the two electrodes. (b) The experimental setup. The cells are immobilized on the chip surface. The medium is DI water containing SYTOX Green or PI stain.

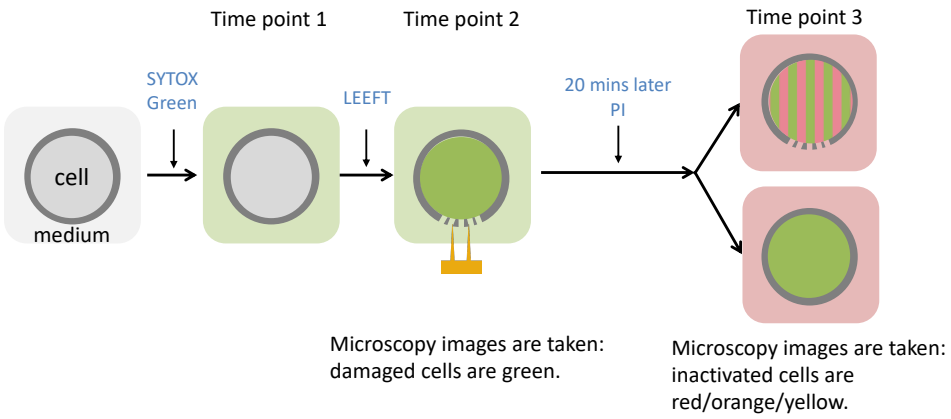

Figure S2. A schematic of the double staining method with SYTOX Green and PI stain.

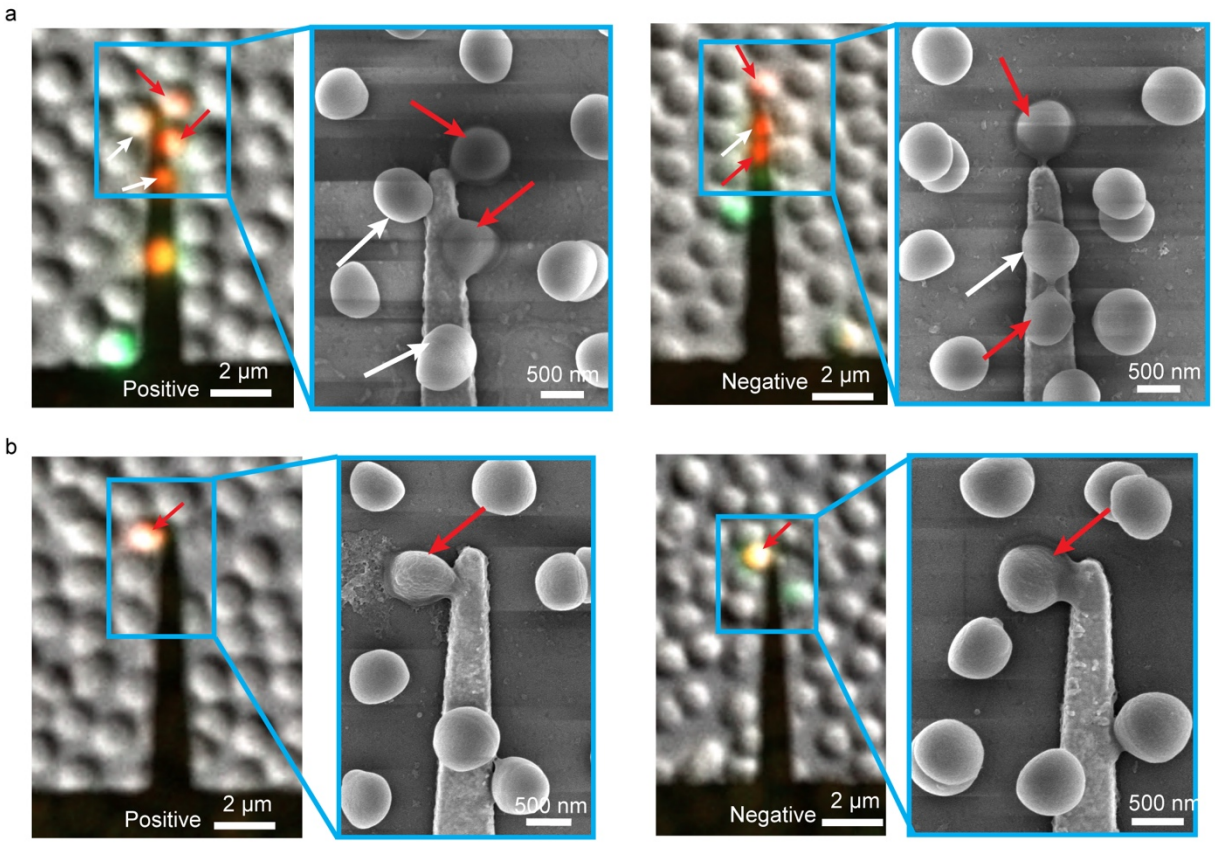

Figure S3. Side-by-side comparison of the optical microscopy images and SEM images for bacteria inactivation by LEEFT using (a) 20 ns pulses at 22 kV/cm with 20 μs effective treatment time and (b) 20 ns pulses at 12 kV/cm with 20 ms effective treatment time.

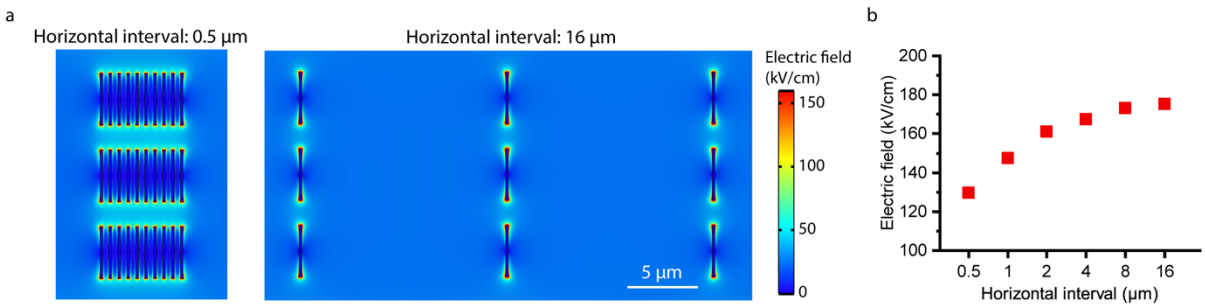

Figure S4. Simulation of the enhanced electric field of nanotip structures on chip. (a) Simulation images of the nanotip structures on chip with different horizontal interval. (b) The nano-enhanced electric field over the horizontal interval between nanotip structures.

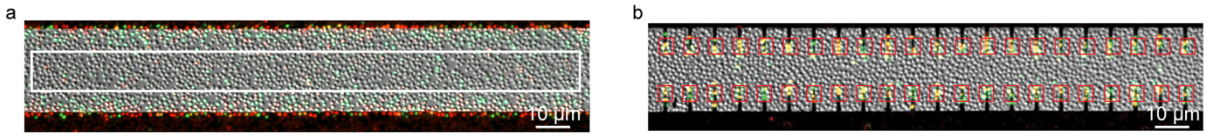

Figure S5. The area of interest for CEFT and LEEFT. (a) The white rectangle is the area of interest for CEFT, which is to investigate the antimicrobial efficiency in the bulk space between the two electrodes. The antimicrobial efficiency of CEFT is calculated as the percentage of cells inactivated or damaged between the two electrodes in the white rectangle. The image was taken after 20 ns pulses at 55 kV/cm for 200 ms effective treatment time. More bacteria are damaged or inactivated at the electrode edge, which is induced by the electric field enhancement due to the thin electrode edge (300 nm thick). However, in practical applications, the electrodes are two parallel plates, where there is no sharp edge and significant electric field enhancement. So, the area of interest (white rectangle) is defined to consider the bulk space and avoid the area affected by the edge. (b) The nanowedge tips are the effective zones of LEEFT, so that the red squares are the area of interest for LEEFT. The antimicrobial efficiency of LEEFT is represented by the percentage of nanowedges inducing bacteria damage or inactivation, which is calculated by the number of nanowedges have damaged/dead bacteria at the tip after treatment divided by the total number of nanowedges. The image was taken after 20 ns pulses at 40 kV/cm for 200 ns effective treatment time.

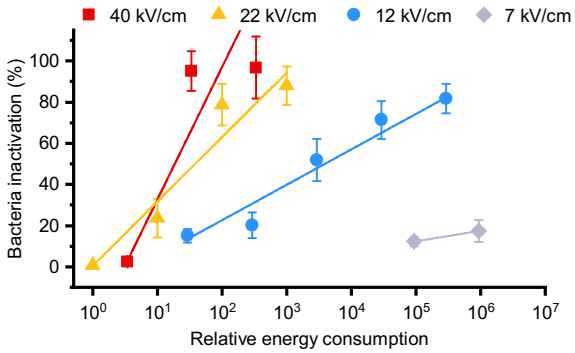

Figure S6. Relative energy consumption of 20 ns pulses at different applied electric field. The energy consumption J is calculated by $J = n\int_{t_1}^{t_2} VI(t)dt$, where V is the applied voltage, I is the current, t_1, t_2 is the starting and ending time of one pulse, t is time, and n is the pulse number. The relative energy consumption is calculated by normalizing all data to the smallest J value. Data are presented as mean values. Error bars represent the s.d. from n = 3 replicates.

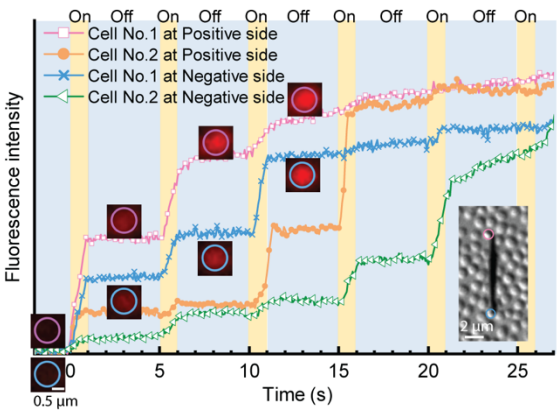

Figure S7. PI fluorescence intensity indicating quick pore closure in the cells located at the tips of non-connected nanowedges. The "on" (yellow area) indicates 20 ns pulses at 12 kV/cm for 1 s. The "off" (blue area) indicates 0 V for 4 s. The insets are optical microscopy images of the cell.

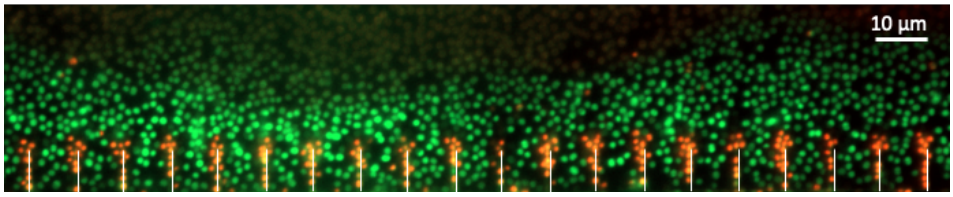

Figure S8. The stack fluorescence microscopy image of DCFH-DA stained cells (green, indicating oxidative stress) and PI stained cells (red, indicating cell inactivation) after LEEFT of 20 ns/500 kHz at 22 kV/cm for 20 ms effective treatment time. The green cells have oxidative stress, but not all of them are inactivated. This indicates that even significant oxidative stress is detected in some cells, it does not necessarily cause bacteria inactivation.

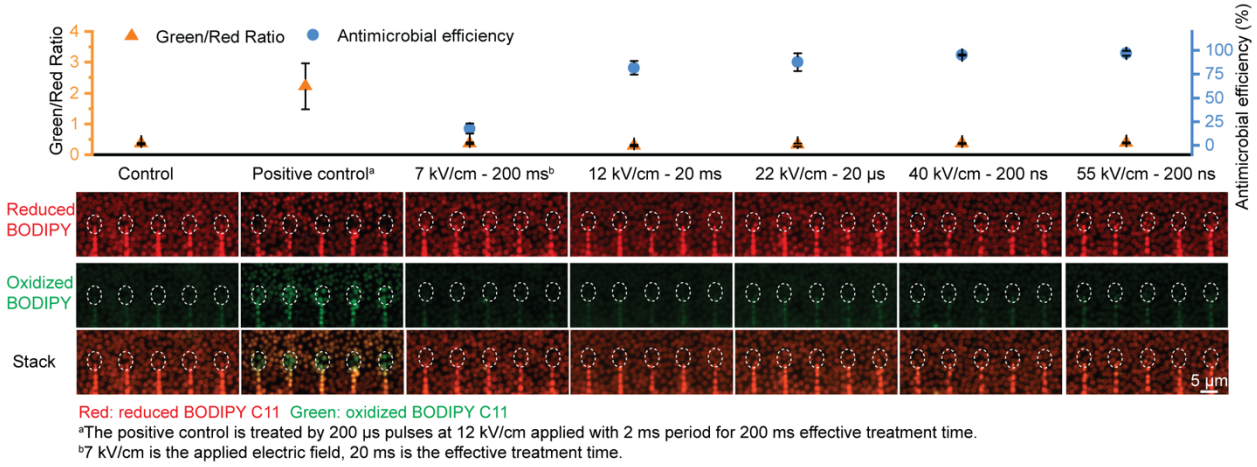

Figure S9. Analysis and microscopy imaging of cell membrane peroxidation under 20 ns pulse treatment. To assess lipid peroxidation, *S. staphylococcus* were stained with 20 µM BODIPY 581/591 C11 reagent and then treated with 20 ns pulses at several different applied electric field and effective treatment times. In the presence of lipid peroxides, the stained cells will show a green shift in fluorescence activity from red at ~590 nm to green at ~510 nm. The Green/Red Ratio is calculated by averaging the green/red fluorescence of 10 cells located exactly at the tip of 10 nanowedge. Higher ratio indicates more sever lipid peroxidation. The results show that the cell Green/Red Ratio after treated with 20 ns pulses stays the same with the control group, which are significantly lower than the positive control group, indicating that no significant lipid peroxidation is detected under 20 ns pulses. The corresponding antimicrobial efficiencies are the same as the data shown in **Figure 2d**. No significant membrane peroxidation is detected even though around 90% bacteria inactivation is achieved, indicating that the bacteria inactivation is not due to extracellular ROS generation or membrane peroxidation. Data are presented as mean values. Error bars represent the s.d. from $n = 3$ replicates.

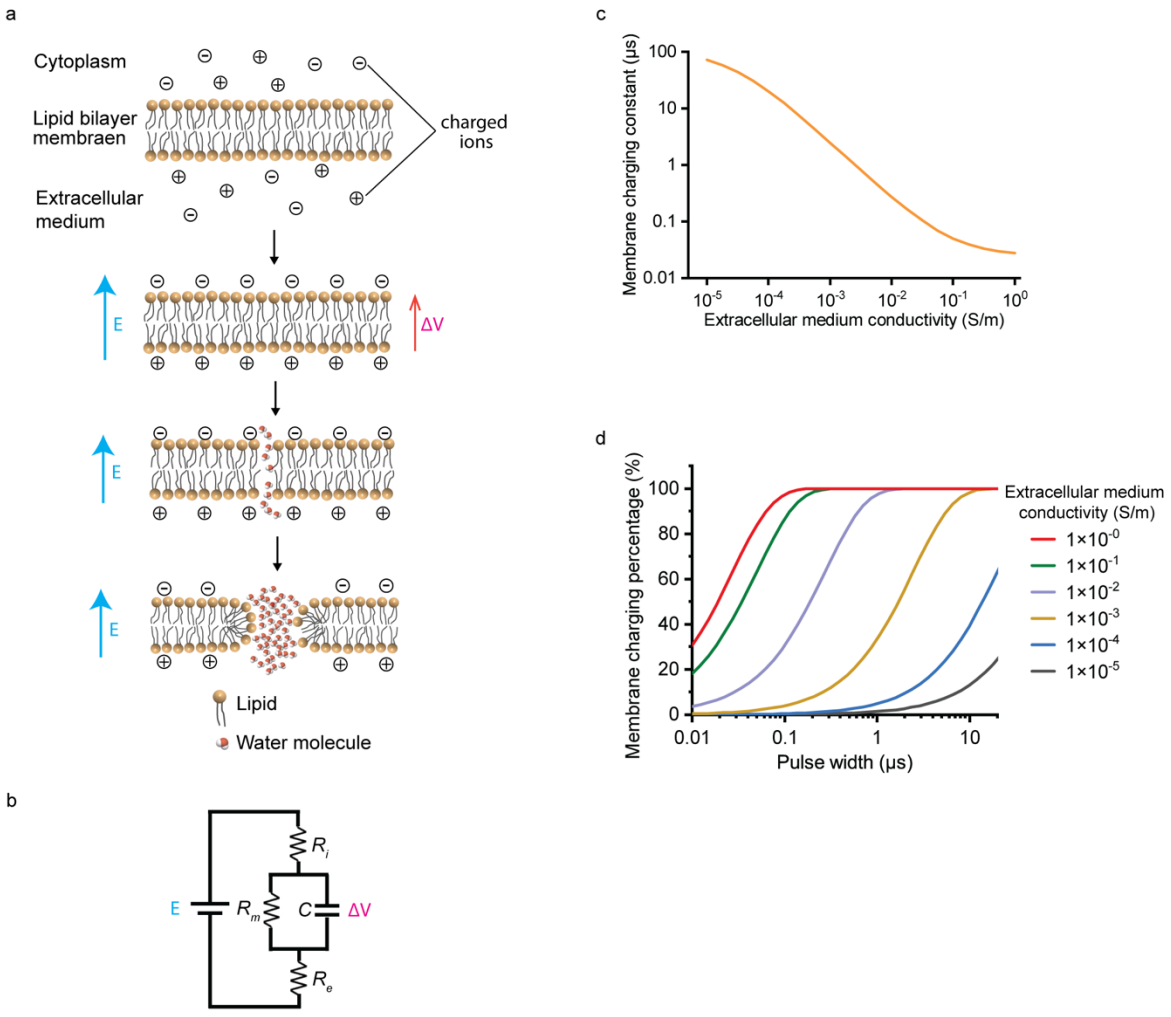

Figure S10. Electroporation process and membrane charging speed analysis. (a) A schematic of the electroporation process. When the lipid bilayer membrane is exposed to an external electric field *E*, charged ions accumulate on the two sides of the membrane, generating an induced TMV (*ΔV*). Then, water molecules orient their dipoles along the transmembrane voltage, forming a water column across the lipid bilayer. The lipids will rearrange their hydrophilic head group toward the water column, generating the hydrophilic pore. (b) The equivalent electrical circuit of the cell membrane charging. R_i, R_e, R_m, and C is the resistance of cytoplasm, extracellular medium, membrane, and the capacitance of the membrane. (c) The relationship between the membrane

charging constant τ and the extracellular medium conductivity σ_e. (d) The dependence of the membrane charging percentage on the pulse width under different medium conductivities.

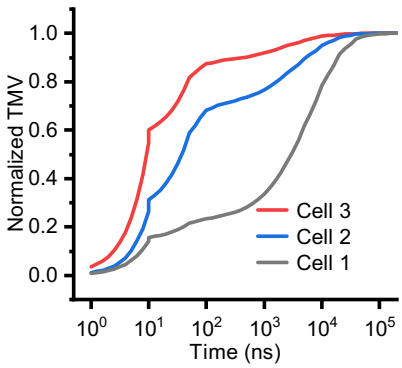

Figure S11. The normalized TMV representing the charging ratio changed with charging time.

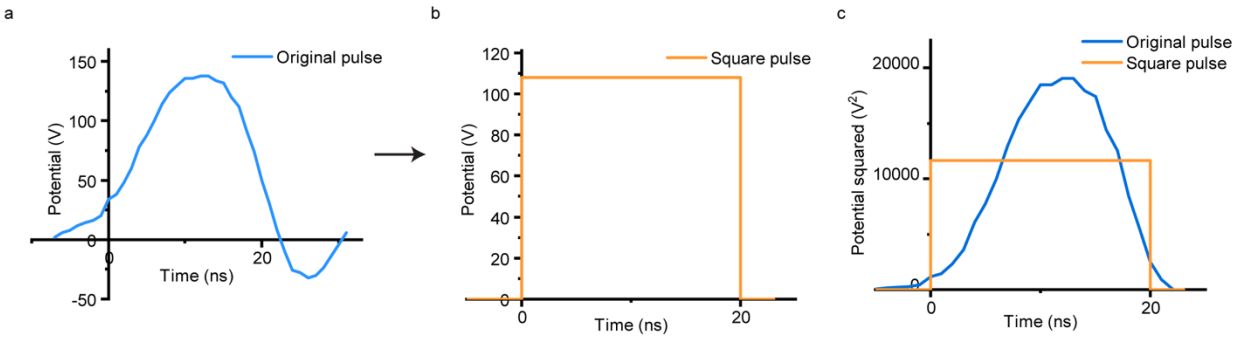

Figure S12. Waveform of a single electrical pulse. (a) The original pulse is a peak due to the short pulse width. (b) The peak is represented as a square pulse at the root mean square (RMS) voltage, which is 108.1 V (22 kV/cm when applied to 50 μm). (c) The RMS voltage is calculated by the equation $V_{\mathrm{RMS}} = \sqrt{\frac{1}{T}\int_{t_1}^{t_2} V^2(t)dt}$, where T is 20 ns, t_1, t_2 are the starting and ending time of the peak, V is potential, and t is time. The area under the original pulse voltage square (blue line) equals to the area under square pulse voltage square (orange line).

REFERENCES

1. Maher, M.; Pine, J.; Wright, J.; Tai, Y.-C., The neurochip: a new multielectrode device for stimulating and recording from cultured neurons. *Journal of neuroscience methods* **1999,** *87*, (1), 45-56.
2. Rojas-Chapana, J. A.; Correa-Duarte, M. A.; Ren, Z.; Kempa, K.; Giersig, M., Enhanced introduction of gold nanoparticles into vital acidothiobacillus ferrooxidans by carbon nanotube-based microwave electroporation. *Nano Letters* **2004,** *4*, (5), 985-988.
3. Howe, K. J.; Crittenden, J. C.; Hand, D. W.; Trussell, R. R.; Tchobanoglous, G., *Principles of water treatment*. John Wiley & Sons: 2012.
4. Katsuki, S.; Xiao, S.; Joshi, R. P.; Laroussi, M.; Schoenbach, K. H. In *Electrical breakdown of sub-millimeter water gaps*, Conference Record of the Twenty-Fifth International Power Modulator Symposium, 2002 and 2002 High-Voltage Workshop., 2002; IEEE: 2002; pp 199-202.
5. Schoenbach, K.; Kolb, J.; Xiao, S.; Katsuki, S.; Minamitani, Y.; Joshi, R., Electrical breakdown of water in microgaps. *Plasma Sources Science and Technology* **2008,** *17*, (2), 024010.
6. Kotnik, T.; Bobanović, F.; Miklavc̆Ic̆, D., Sensitivity of transmembrane voltage induced by applied electric fields—A theoretical analysis. *Bioelectrochemistry* **1997,** *43*, (2), 285-291.
7. Icier, F.; Ilicali, C., The effects of concentration on electrical conductivity of orange juice concentrates during ohmic heating. *European Food Research and Technology* **2005,** *220*, (3), 406-414.